Available online at www.sciencedirect.com

ScienceDirect

IFAC PapersOnLine 55-27 (2022) 208–213

Design of The CRONE Automatic Headlight Leveling System

Safouane El Khadri[1,2,3], Xavier Moreau[2,3], André Benine-Neto[2,3], Mathieu Chevrié [2,3], Whilk Marcelino Gonçalves[1,3] and Franck Guillemard[1,3]

[1]*Stellantis, 78140 Vélizy-Villacoublay, France (e-mail: firstname.lastname@stellantis.com)*
[2]*Laboratory IMS, UMR 5218 CNRS, University of Bordeaux, 33405 Talence, France (e-mail: firstname.lastname@ims-bordeaux.fr)*
[3]*OpenLab Electronics and Systems for Automotive combining Stellantis and IMS Laboratory*

Abstract: Automotive headlights system represents a safety key system when it comes to drive by night. It aims to increase the comfort of the driver by providing a clear visibility in order to anticipate obstacles and follow the right path. One of the main challenges that the lighting system is facing today is its automatic leveling adjustment. Variations of load of the vehicle, its dynamics and the environment are the main sources of disturbance to the leveling system. These disturbances causes variations of vehicle pitch angle and as a result the lighting cut-off level that may glare other road users and affect the driver's visibility range. This paper proposes an innovative automatic leveling system based on an ultrasonic motor which is able to dynamically reject such disturbances on the lighting cut-off level using a robust CRONE controller.

Keywords: Headlight systems, piezoelectric motor, glare, CRONE, robust control, Matrix Beam, leveling system, ADB.

1. INTRODUCTION

The evolution of automotive lighting systems is going in an exponential pace with the emergence of the autonomous vehicle, which is equipped with intelligent sensors. The front camera is the main sensor on which relies the recent lighting systems and is the key behind several innovations. The main ones were the introduction of the adaptive lighting systems and the Matrix beam (Elger et al., 2013).

The Matrix Beam is a headlight system containing multiple light sources, which enables the control of different parts of the illuminated scene independently. This allows a multitude of possibilities of lighting adjustment according to several scenarios. The main use case is to allow the driver to use the high beam even when crossing or following other road users.

Fig. 1 illustrates the added value of the Matrix Beam system (Fig. 1.b) over a common lighting system (Fig. 1.a). The Matrix Beam system increases the environment visibility without glaring the vehicle in front.

(a) (b)

Fig. 1. (a) Conventional low beam with limited visibility, (b) The Matrix Beam system, enables the Glare Free High Beam (GFHB) function that illuminates the environment without the upper car body to avoid glare (photo: HELLA)

Compared to a regular headlamp system, the Matrix Beam module structure benefits from a large number of LEDs placed horizontally which provides a wider opening angle horizontally. Such feature also enhances the functionality known as 'bending light' in which the beam direction and width are adapted according to the steering angle.

Nevertheless, the low beam cut-off must be kept stable vertically in order to avoid glare. The matrix beam, using multiple rows also requires a stable vertical aiming to be precise enough. For this reason, leveling systems are mandatory to adapt the position of the vertical aiming position to the right level according to the regulation ECE R48 (UNITED NATIONS, 2021 (see references)).

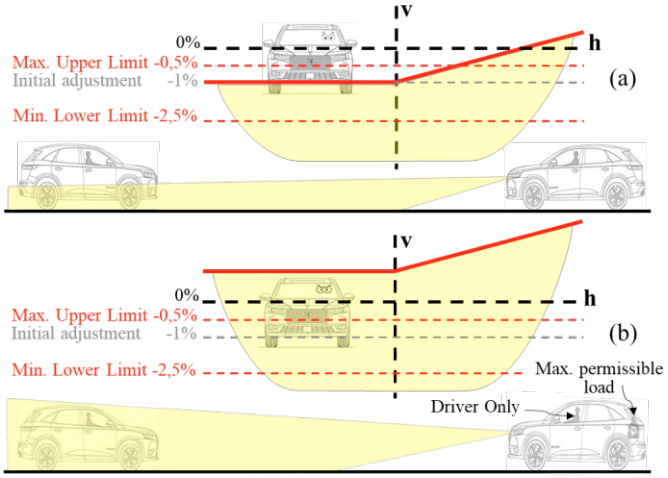

Fig. 2. (a) Optimal lighting cut-off line position according to the regulation, (b) Influence of static loading conditions on the cut-off line position

10.1016/j.ifacol.2022.10.513

This regulation obligates to control the position of headlamps according to the vehicle load. As it is illustrated in Fig. 2, the cut-off line must be as shown in Fig. 2.a, in order to guarantee a good range of visibility and to not glare other road users as it occurs in Fig. 2.b, where the load of the vehicle engendered a variation of pitch angle raising the cut-off line of the lighting and thus causing glare.

By respecting the regulation of ECE, the glare issue is partially solved, but when facing some temporary scenarios, as illustrated in Fig. 3 the driver can lose some visibility range and may glare other road users.

These additional scenarios are important as they increase safety and comfort of road users. The headlight leveling system that corrects these disturbances should be fast and eco-friendly.

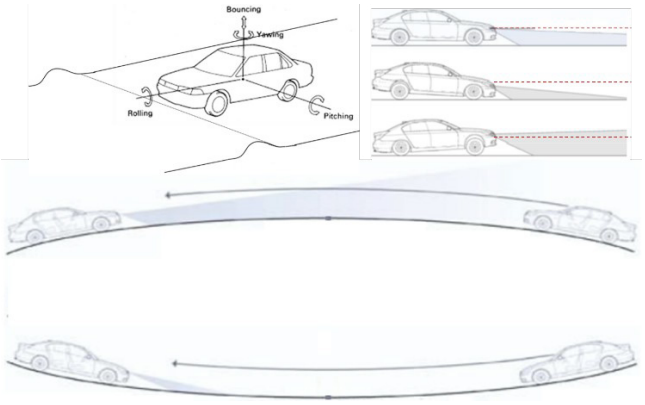

Fig. 3. Examples of non-covered scenarios by ECE R48

1.1 Conventional headlight leveling systems

A common leveling system (Valeo service, 2015), as shown in Fig. 4, includes leveling sensors, Electronic Control Unit (ECU) and an actuator on each headlamp that controls the position of the cut-off line. DC motor is used to regulate the position of the headlamp according to the load when starting the vehicle, whereas stepper motors covers additional scenarios when the vehicle is moving. These two solutions satisfy the regulation ECE R48. However, it could not be used to cover the scenarios in Fig. 3 showing that other road users may be glared by the light beam, when the vehicle is crossing the top of a hillock. A significant loss of visibility may likewise occur when crossing the bottom of a hollow.

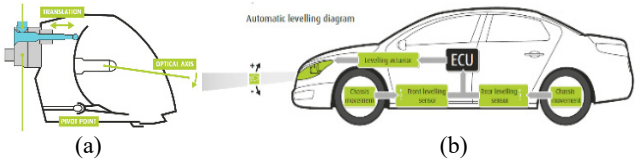

(a) (b)

Fig. 4. (a) Motorized leveling system working principle, (b) Common headlamp leveling solution

1.2 Innovative solution for headlight leveling system

In order to adapt the leveling system to the use cases from Fig. 3, the usage of a fast-dynamic response actuator and sensor is needed. The so-called ultrasonic motor (Wallaschek, 1995) (see Fig. 5.b) is an adequate actuator, as in comparison with electromagnetic motors, it provides: faster responses; higher torque in low speed and holding torque without power supply. Moreover, it occupies less volume, it is less influenced by electromagnetic interferences, and it is a low consumption energy component.

For the sensing part, as illustrated by Fig. 5.a, the usage of a MEMS sensor composed from a 3-axis gyroscope and accelerometer provides the system with precise measurement in real time.

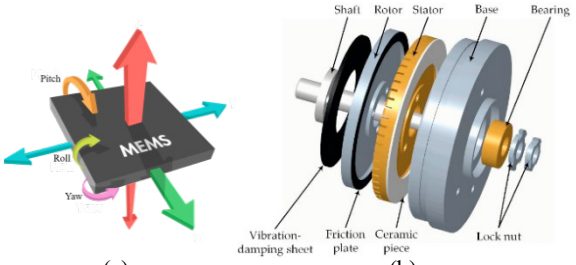

(a) (b)

Fig. 5. (a) MEMS sensor, (b) Piezoelectric motor structure (Sattel, 2002)

This article proposes the vertical control of the beam for a leveling system equipped with a piezoelectric motor. The next sections are organized as follows: Section 2 describes the automatic headlight leveling system. The design of a simulator from a piezoelectric motor (USR60) and the vehicle dynamics model which causes pitch angle disturbances affecting the optical system are described in Section 3. The linearization of the actuator system with uncertainties is also presented. Such step is key for the controller design in frequency domain which is addressed in Section 4. Simulations of the proposed headlight leveling controller are described in Section 5. The last section provides conclusions and prospects.

2. SYSTEM DESCRIPTION

The Automatic Headlight Leveling System (AHLS) presented in Fig. 6 consists of a $\varphi_{ref}(t)$ reference generator, a $u_c(t)$ feedback control and a headlamp with its actuator. $\varphi_h(t)$ is the headlight angular position, $n_m(t)$ a measurement noise and $\varepsilon(t)$ the error signal.

Note that the robust controller is designed with the CRONE Control-System Design (CSD) methodology that is a frequency-domain approach (Oustaloup, 2014).

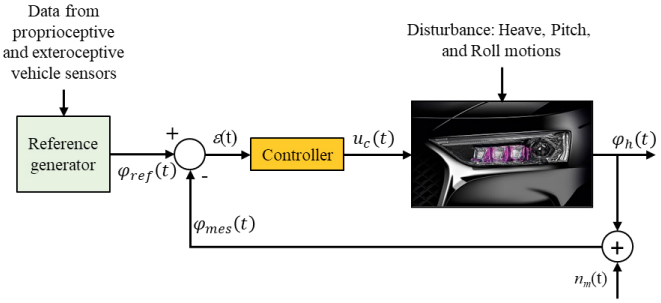

Fig. 6. Block diagram of the AHLS

3. SYSTEM MODELING

In order to assess the AHLS controller performances in time domain, a simulator composed of vehicle dynamics and motored headlight dynamics is necessary. The vehicle dynamic model is used to generate disturbances which are applied to the AHLS. Note that the dynamic model of the motored headlight system is firstly used to analyze and to understand its dynamic behavior, and then to design the automatic control system.

3.1 Vehicle model

The AHLS is linked to the chassis. This is why the angular position $\varphi_h(t)$ of the headlights with respect to a horizontal reference plane is disturbed by the movement of the chassis (heave, pitch, and roll) resulting from road and driver inputs. It is therefore necessary to consider the dynamics of the vehicle when designing the AHLS.

Fig. 7 illustrates the causal link between vehicle dynamics and headlamp.

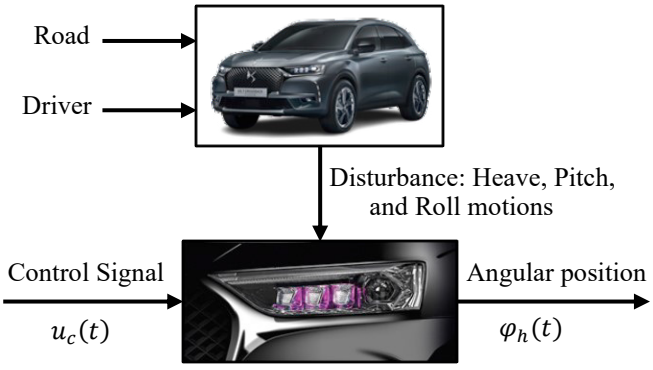

Fig. 7. Illustration of the causal link between vehicle dynamics and headlamp

In this study, a 4-wheel car model with 14 degrees of freedom is used to simulate the vehicle dynamics (Schramm et al., 2014). Note that the natural frequencies associated with heave, pitch, and roll motions are around 1.2 Hz for a passenger car. For this reason, the spectral content of the disturbance applied to the automatic headlight leveling system and resulting from the movement of the chassis is considered around 1.2 Hz.

3.2 Piezoelectric motor

In order to control the angular position $\varphi_h(t)$ of each headlight, a traveling wave piezoelectric motor is considered for the AHLS. The piezoelectric motor is a complex system due to non-linearity caused mainly by the piezoelectric material characteristics. The model of such an actuator is derived from (Bullo, 2005) and (Brahim, 2017).

Fig. 8 and Fig. 9 show an inside view and the block diagram of traveling wave piezoelectric motor respectively.

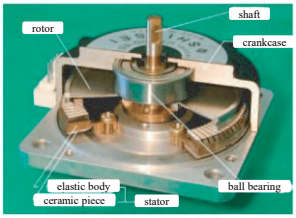

Fig. 8. Inside view of traveling wave piezoelectric motor (Bullo, 2005)

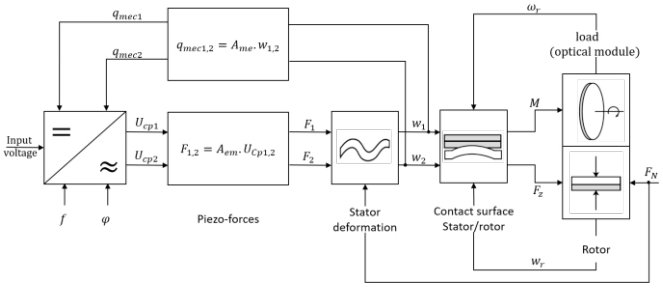

Fig. 9. Block diagram of traveling wave piezoelectric motor (Bullo, 2005)

Without electrical power supply, the rotor is stuck to the stator thanks to an axial preload force F_N, thus ensuring a static holding torque (as a parking brake system). In this case, the contact surface between stator and rotor is annular (see Fig. 8).

When two sinusoidal electric voltages U_{cpi}, with $i = 1$ and 2, at high frequency f and phase-shifted by φ are applied to the piezoelectric stator, two sinusoidal forces $F_i(t)$ appear from piezo effect. The consequence is that two deformations $w_i(t)$ are created and give rise to a traveling wave $w_r(t)$ at the surface of the stator. This wave creates a force $F_z(t)$ that overcomes the preload force F_N in order to free the rotor. In this case, the initial annular contact surface between the stator and the rotor is reduced to several points due to the deformation wave propagation of the stator. From this instant, the rotor starts to move with an angular speed $\omega_r(t)$. This motion is due to frictional force at contact points resulting from the deformation wave propagation.

The rotor movement control is obtained from the control signal $u_c(t)$ (input voltage), the frequency f and the phase-shift φ applied to the static convertor (see Fig. 9). In (Brahim, 2017), a sensitivity analysis is proposed to show the impact of each variable $u_c(t)$, f, and φ upon the rotor movement.

In this paper, the input frequency f is set to 40 kHz in order to operate at best efficiency (Bullo, 2005), and the phase-shift φ is set to $\pm\frac{\pi}{2}$ depending on the desired rotation direction.

3.3 Linearized model of the plant

In order to design the CRONE controller in frequency domain, a linearized model of the plant is derived around the operating point fixed by $\varphi_h^e = \varphi_{ref} = 0$. The main static non-linearity of the plant is linked to the stator deformation due to the direct and indirect piezoelectric effects, and due to the non-linear

behavior of the frictional force at contact points between stator and rotor. For controller design, this non-linearity is interpreted as an uncertain bounded linear gain K_{pe}, with $K_{pe} \in \left[\underline{K_{pe}} \; ; \; \overline{K_{pe}}\right]$. In this case, the relation between the torque $M(t)$ developed by the actuator and the control signal $u_c(t)$ is given by:

$$M(t) = K_{pe}\, u_c(t)\,. \tag{1}$$

Moreover, the behavior analysis of the actuator from the simulator reveals that the dynamics of piezoelectric part and that of stator deformation propagation part are very fast comparing to the rotational dynamics of the rotor. That is why the fast dynamics are neglected during controller design. The rotational dynamics of the rotor is defined by:

$$J_{eq}\, \dot{\omega}_{\mathrm{r}}\,(t) = M(t) - T_f(t)\,, \tag{2}$$

where J_{eq} is an uncertain equivalent inertia moment resulting to the inertia moment of the actuator rotor and the headlamp with $J_{eq} \in \left[\underline{J_{eq}} \; ; \; \overline{J_{eq}}\right]$, $T_f(t)$ is a frictional torque given by:

$$T_f(t) = b_{eq}\, \omega_r(t)\;, \tag{3}$$

where b_{eq} is an equivalent viscous frictional coefficient with $b_{eq} \in \left[\underline{b_{eq}} \; ; \; \overline{b_{eq}}\right]$. Note that the mechanical transmission between the actuator and the headlamp is direct (no speed reducer), that is why:

$$\dot{\phi}_h(t) = \omega_r(t)\;. \tag{4}$$

By supposing null initial conditions, the Laplace transform of equations (1) to (4) leads to the transfer function between the angular position $\bar{\varphi}_h(s)$ and the control signal $U_c(s)$, namely:

$$G(s) = \frac{\bar{\varphi}_h(s)}{U_c(s)} = \frac{K_0}{s\left(1 + \dfrac{s}{\omega_0}\right)}\;, \tag{5}$$

where $K_0 = K_{pe}/b_{eq}$ is an uncertain gain with $K_0 \in \left[\underline{K_0} \; ; \; \overline{K_0}\right]$ and $\omega_0 = b_{eq}/J_{eq}$ an uncertain transitional frequency with $\omega_0 \in \left[\underline{\omega_0} \; ; \; \overline{\omega_0}\right]$. For the design of robust controller, three cases are considered:

- a nominal case 0 defined by $G_0(s, K_0, \omega_0)$;

- two extremal cases 1 and 2 defined by $G_1\left(s, \underline{K_0}, \overline{\omega_0}\right)$ and $G_2\left(s, \overline{K_0}, \underline{\omega_0}\right)$.

Table 1 gives the different numerical values of K_0 and ω_0.

Table 1: Numerical values of K_0 and ω_0

Parameters	Nominal	Min	Max
K_0 [rad.(s V)$^{-1}$]	100	60	167
ω_0 [rad/s]	3.87	2.64	5.38

Fig. 10 presents the Bode plots of $G_0(\mathrm{j}\omega)$, $G_1(\mathrm{j}\omega)$, and $G_2(\mathrm{j}\omega)$ obtained with numerical values of Table 1.

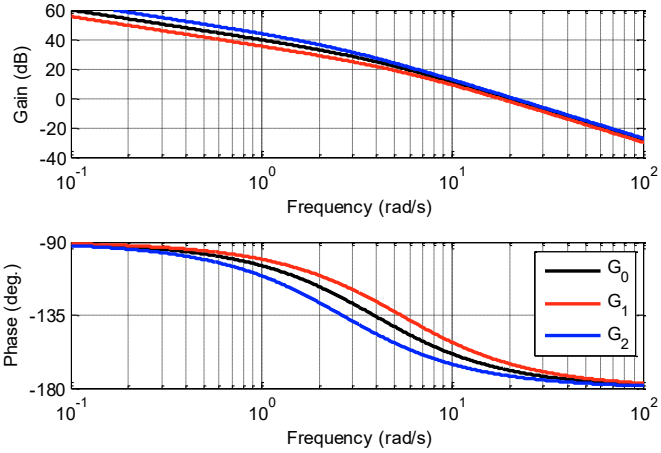

Fig. 10. Bode plots of $G_0(\mathrm{j}\omega)$, $G_1(\mathrm{j}\omega)$ and $G_2(\mathrm{j}\omega)$

4. CONTROLLER DESIGN

4.1 Control design specifications

The design specifications for the AHLS controller are the following:

- a phase margin $M_\phi \geq 45°$;
- an open-loop gain crossover frequency $\omega_u \geq 2\pi 10$ rad/s;
- a steady-state error equal to 0;
- a variation range of u_c given by $-12\ V \ \leq \ u_c \leq \ 12\ V$.

4.2 CRONE Control-System Design (CSD) methodology

The CRONE CSD methodology is a frequency-domain approach which is being developed since the 80's. It is based on the common unity-feedback configuration presented in Fig. 10. Three CRONE CSD methods have been developed, each one of them denotes a generation of CRONE design. The general form of the nominal open-loop transfer function $\beta_{nom}(s)$ of the second-generation CRONE control is defined by:

$$\beta_{nom}(s) = \beta_0 \left(\frac{1 + s/\omega_l}{s/\omega_l}\right)^{n_l} \left(\frac{1 + s/\omega_h}{1 + s/\omega_l}\right)^{n} \left(1 + \frac{s}{\omega_h}\right)^{-n_h}, \tag{6}$$

where the first part of (6) represents the behavior at low frequencies with an integer order n_l, the second represents the behavior at middle frequencies around ω_u with n the fractional order between 1 and 2, and the last represents the behavior at high frequencies with an integer order n_h. As for the gain β_0, it is defined by:

$$\beta_0 = \left(\frac{\omega_u}{\omega_l}\right)^{n_l} \left(1 + \left(\frac{\omega_u}{\omega_l}\right)^2\right)^{\frac{n-n_l}{2}} \left(1 + \left(\frac{\omega_u}{\omega_h}\right)^2\right)^{\frac{n_h-n}{2}}. \tag{7}$$

With a phase margin $M_\phi = 45°$, $\omega_u = 2\pi 10$ rad/s and in accordance with the methodology described in (Lanusse et al., 2013), the values of the parameters from the open-loop transfer function are:

$$\begin{cases} n_l = 2\ ,\ n = 1.5\ ,\ n_h = 3 \\ \omega_l = 1.13 \text{ rad/s}\ ,\ \omega_h = 3487 \text{ rad/s}\ ,\ \beta_0 = 412.3. \end{cases}$$

Once the nominal open-loop transfer is determined, the fractional controller $C_F(s)$ is defined by its frequency response:

$$C_F(\mathrm{j}\omega) = \beta_{nom}(\mathrm{j}\omega)/G_{nom}(\mathrm{j}\omega), \quad (8)$$

the synthesis of the ideal frequency response $C_F(\mathrm{j}\omega)$ consists of identifying a rational frequency response $C_R(\mathrm{j}\omega)$ given by:

$$C_R(\mathrm{j}\omega) = B(\mathrm{j}\omega)/A(\mathrm{j}\omega), \quad (9)$$

where $B(\mathrm{j}\omega)$ and $A(\mathrm{j}\omega)$ are polynomials of specified integer degrees n_B and n_A . Any frequency-domain system identification techniques can be used (Lanusse, 1994).

Fig. 11 presents the Bode plots of the controller $C_R(\mathrm{j}\omega)$.

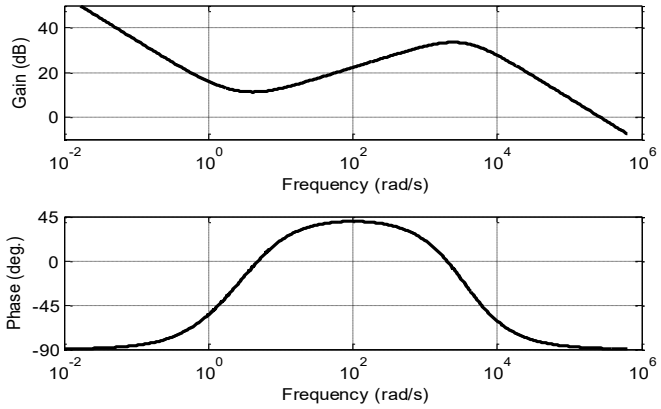

Fig. 11. Bode plots of $C_R(\mathrm{j}\omega)$

5. SYSTEM PERFORMANCE

5.1 Frequency domain

Fig. 12 presents the Bode plots (a) and the Nichols loci (b) of the open-loop transfer function $\beta(\mathrm{j}\omega)$, the Bode plots of complementary sensitivity function $T(\mathrm{j}\omega) = \frac{C_R(\mathrm{j}\omega)G(\mathrm{j}\omega)}{(1+C_R(\mathrm{j}\omega)G(\mathrm{j}\omega))}$ (c), of sensitivity function $S(\mathrm{j}\omega) = \frac{1}{1+C_R(\mathrm{j}\omega)G(\mathrm{j}\omega)}$ (d) obtained with the CRONE controller for the three cases (0, 1, 2). As one can observe, the phase margin M_ϕ (b) and the resonant peaks Q_T of $T(\mathrm{j}\omega)$ (c) and Q_S of $S(\mathrm{j}\omega)$(d) remain constant for all the cases thus showing the robustness of the stability degree (Lanusse, 2010).

5.2 Time domain

The scenario used to validate the AHLS in time domain (with the simulator described in section 3) is defined by a vehicle moving in a straight line on a horizontal road at a constant speed of 30 km/h and crossing a speed bump 10 cm high (Fig. 13.a).

For this scenario, the disturbance applied to the AHLS is the pitch angle $\varphi_p(t)$ of the chassis.

Fig. 13.a presents time responses of the reference angle $\varphi_{ref}(t)$, the headlight angle $\varphi_h(t)$, and the pitch angle $\varphi_p(t)$ of the chassis (disturbance) (b), the error signal $\varepsilon(t)$ (c) and the control signal $u_c(t)$ (d).

It is possible to note that the AHLS ensures a good rejection of the disturbance $\varphi_p(t)$ with a control signal $u_c(t)$ that remains within the variation range defined by -12V and 12V. Note that without the AHLS, the angle $\varphi_h(t)$ would be equal to the angle $\varphi_p(t)$.

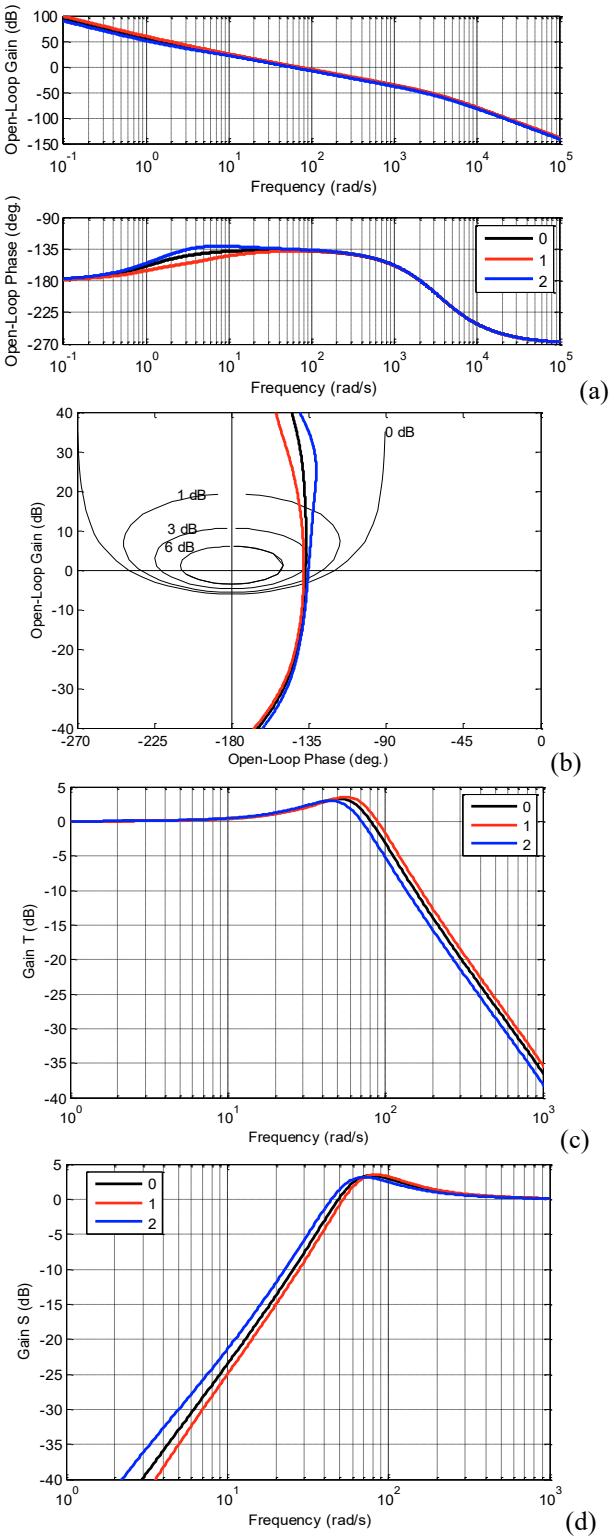

Fig. 12. Bode plots (a) and Nichols loci (b) of $\beta(\mathrm{j}\omega)$, $T(\mathrm{j}\omega)$ (c) and of $S(\mathrm{j}\omega)$ (d) for the nominal case 0 (in **black**) and the extremal cases 1 (in **red**) and 2 (in **blue**)

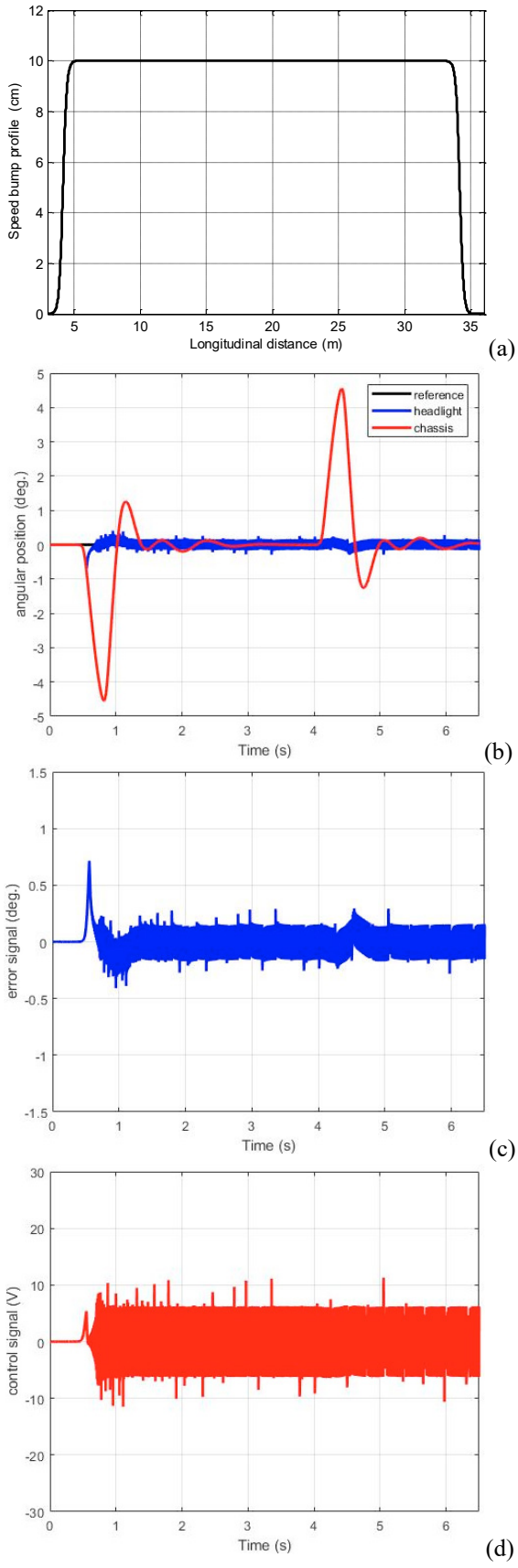

Fig. 13. Speed bump profile (a), time responses of $\varphi_{ref}(t)$ (in **black**), $\varphi_h(t)$ (in **blue**) and $\varphi_p(t)$ (in **red**) (b), error signal $\varepsilon(t)$ (c) and control signal $u_c(t)$(d)

6. CONCLUSION

In this paper, an Automatic Headlight Leveling System using an ultrasonic motor and a second-generation CRONE controller has been proposed.

This AHLS has been put on the test in simulation and shown a good rejection of disturbances that cause variations of the lighting cut-off level.

In future works, authors intend to deal with the design of a third generation CRONE controller and H_∞ controller for comparison with the presented controller in this paper. Another major step will be to implement the AHLS on hardware components and assess its effectiveness on a real test bench.

ACKNOWLEDGMENT

This work took place in the framework of the OpenLab "Electronics and Systems for Automotive" combining IMS laboratory and Stellantis company.

REFERENCES

Brahim, M. M. (2017) Modeling and Position Control of Piezoelectric Motors, PhD, Gif sur Yvette, France, Université Paris-Saclay.

Bullo, M. (2005) Modélisation et commande du moteur piézoélectrique à onde progressive, PhD, Lausanne, Switzerland, École Polytechnique Fédérale de Lausanne.

Elger, G., Spinger, B., Bienen, N. and Benter, N. (2013) 'LED Matrix Light Source for Adaptive Driving Beam Applications', IEEE 63rd Electronic Components and Technology Conference (ECTC).

Lanusse, P. (1994) De la commande CRONE de première génération à la commande CRONE de troisième generation, PhD, France, Bordeaux I University.

Lanusse, P. (2010) CRONE toolbox [Computer program]. Available at http://www.ims-bordeaux.fr/CRONE/toolbox.

Lanusse, P., Malti, R. and Melchior, P. (2013) 'CRONE control system design toolbox for the control engineering community: Tutorial and case study', Philosophical transactions. Series A, Mathematical, physical, and engineering sciences, vol. 371, no. 1990.

Oustaloup, A. (2014) Diversity and Non-integer Differentiation for System Dynamics, Wiley.

Sattel, T. (2002) Dynamics of Ultrasonic Motors, PhD, University of Darmstadt.

Schramm, D., Bardini, R. and Hiller, M. (2014) Vehicle Dynamics: Modeling and Simulation, Berlin Heidelberg, Springer.

(2021) 'UN Regulation No 48 - Uniform provisions concerning the approval of vehicles with regard to the installation of lighting and light-signalling devices [2021/1718]', in Official Journal.

Valeo service (2015) Valeo Lighting Systems: From light to advanced vision technologies - valeoscope technical handbook, Valeo service.

Wallaschek, J. (1995) 'Piezoelectric Ultrasonic Motors', Journal of Intelligent Material Systems and Structurs, vol. 6.